

Ceramic Nanoparticle-Decorated Melt-Electrospun PVDF Nanofiber Membrane with Enhanced Performance as a Lithium-Ion Battery Separator

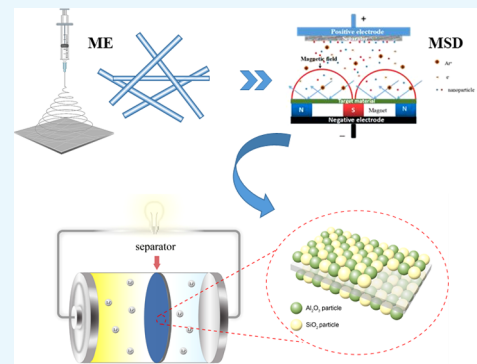
Shuanglin Wu,[†] Jingxia Ning,[†] Feng Jiang,[‡] Jiayi Shi,[†] and Fenglin Huang^{*,†,§,||}

[†]Key Laboratory of Eco-Textiles, Ministry of Education, Jiangnan University, Wuxi 214122, China

[‡]Department of Wood Science, University of British Columbia, Vancouver V6T 1Z4, Canada

[§]Jiangsu Anreda New Materials Limited Company, Changzhou 21300, China

ABSTRACT: Designing a composite separator that can withstand high temperature, deliver high capacity, and offer fast charge–discharge capability is imperative for developing a high-performance lithium-ion battery. Here, a series of ceramic nanoparticle-coated nanofiber membranes, including Al_2O_3 /poly(vinylidene fluoride) (PVDF), SiO_2 /PVDF, and $\text{Al}_2\text{O}_3/\text{SiO}_2$ /PVDF, were prepared by melt-electrospinning and magnetron sputtering deposition. Among all of these composite separators, $\text{Al}_2\text{O}_3/\text{SiO}_2$ /PVDF showed several advantages including excellent thermal stability (no dimensional shrinkage at temperature up to 130 °C and an onset degradation temperature of 445 °C) and superb electrolyte compatibility (340% electrolyte uptake). In addition, the β phase of the fibrous PVDF membrane as well as the presence of polar ceramic nanoparticles on the fiber surface can synergistically improve the ion conductivity to 2.055 mS/cm at room temperature, which is more than 8 times higher than that of the commercial polyethylene (PE) separator. Performance of these ceramic nanoparticle-coated separators in a lithium-ion battery demonstrated an improved discharge capacity of 161.5 mAh/g and more than 84.3% capacity retention rate after 100 cycles. The ceramic nanoparticle-coated PVDF separators also maintained 58.4% capacity at a high current density of 8C, which is better than the 49.8% capacity for the commercial PE separator. Therefore, the ceramic nanoparticle-coated PVDF membrane proves to be a promising separator for a high-power and more secure lithium-ion battery.



1. INTRODUCTION

The lithium-ion battery has witnessed widespread applications ranging from portable electronics to electric vehicles or even electric grids, all benefiting from its high energy density, high power density, long cycle life, and environmental friendliness.¹ The design of the lithium-ion battery includes a cathode, an anode, and a separator, where the separator is a critical component that separates the anode from the cathode to prevent short circuit while allowing rapid transport of lithium ions in the liquid electrolyte.² To date, most commercial separators are made from polyolefin membranes. Although these membranes are characterized with excellent mechanical strength and chemical stability, they also suffer from severe disadvantages such as low porosity (about 40%), poor electrolyte wettability, low thermal stability, and unidirectional mechanical integrity.^{2,3}

Poly(vinylidene fluoride) (PVDF) has recently been investigated for a lithium-ion separator due to its superior film properties as compared to polyolefin ones, including good electrolyte affinity, excellent thermal stability, and superb electrochemical performances.⁴ Other than these excellent physical properties, the β phase (TTTT) of the PVDF crystal shows the highest polarity and dielectric constant among all five crystal phases of PVDF,⁵ which can benefit the ionization of lithium salt in the electrolyte, thereby increasing the lithium ion

concentration in the electrolyte and improving the ionic conductivity. It has also been reported that both strong electric field and high temperature are favorable for the growth of the β phase.^{6,7} Therefore, it is significant to explore a film-forming strategy that can provide both high temperature and strong electric field.

Recently, electrospinning has been widely used in fabricating nanofibrous membranes for lithium-ion battery separator applications,^{8–10} as electrospinning can offer membranes with favorable characteristics such as controllable fiber diameter, large specific surface area, and high porosity, which will necessarily lead to high electrolyte absorption and retention rate, as well as improved lithium ion conductivity. In general, electrospinning can be performed using either polymer melts or polymer solutions.¹¹ In comparison, melt-electrospinning (ME) is more economical and environmentally friendly due to the absence of organic solvents and the simplicity of the process.^{12,13} In addition, as introduced previously, the high temperature and strong electric field during melt-electrospinning can favor the growth of the β phase of PVDF, which is hypothesized to

Received: May 27, 2019

Accepted: September 19, 2019

Published: September 27, 2019

improve the electrochemical performance of the PVDF separator.

Coating commercial lithium-ion battery separators with ceramic layers, such as SiO_2 , Al_2O_3 , ZrO_2 , TiO_2 , and CeO_2 ^{14–19} has been extensively explored as an effective and economic way to improve the thermal stability and wettability of the separator. However, the conventional ceramic coating can also lead to several intrinsic disadvantages. First, the ceramic coating can block separator pores, resulting in poor electrolyte permeability and increased internal resistance of batteries.^{20–22} Second, the ceramic-coated separator consumes more than 20% binders that leads to increased production cost.²³ In addition, the large thickness of the ceramic layer, ranging from 3 to 20 μm , can increase the transfer resistance of the composite separator.²⁴ To address these problems, we propose a simple and feasible method, magnetron sputtering, to deposit ceramic nanoparticles onto the surface of the separator. Magnetron sputtering deposition (MSD) has been demonstrated as an effective surface modification method with a precise control of the nanoparticle shape, size, and distribution by adjusting the process parameters, such as power, pressure, and deposition time.^{25,26}

Herein, we successfully fabricate a novel fibrous separator by melt-electrospinning and magnetron sputtering. It is hypothesized that melt-electrospinning can introduce both high temperature and strong electric field to induce the growth of the β phase in the PVDF membrane. In addition, magnetron sputtering can grow nanometer-thick ceramic nanoparticle layers on PVDF fibers, which can further enhance electrolyte and lithium electrode affinity. By means of melt-electrospinning and magnetron sputtering, the as-fabricated ceramic nanoparticle-coated membrane showed improved thermal stability, electrolyte uptake and affinity, lowered impedance, and interfacial resistance, as well as enhanced discharge capacity and cycling performance in the lithium-ion battery.

2. RESULTS AND DISCUSSION

2.1. Morphological and Chemical Analyses of Membranes. Fourier transform infrared (FTIR) spectra of both the PVDF pellet and melt-electrospun membrane were acquired to investigate the effect of temperature and electric field on the crystalline-phase transformation. Both spectra showed the characteristic absorption peaks at 1186, 976, 876, 796, 765, and 615 cm^{-1} , associated with the α crystalline phase of PVDF, as well as those at 1279, 1074, and 840 cm^{-1} , associated with the β phase of PVDF.²⁷ Compared to the spectrum of the PVDF pellet, the peaks at 1148 and 850 cm^{-1} associated with the α phase disappeared in ME-PVDF, whereas the intensities of other α -phase peaks at 976, 796, 765, and 615 cm^{-1} decreased significantly. In addition, it clearly showed that the β -phase peaks at 1279 and 840 cm^{-1} increased significantly after the melt-electrospun treatment. At operating temperature above the melting point of PVDF, the crystal phase in PVDF pellets starts to melt and the molecular chain mobility increases with the increase of temperature;²⁸ under the action of the electric field, the rotation of the molecular chain and the orientation of the intrinsic dipoles lead to the all-trans plane zigzag conformation, thereby increasing the PVDF β -phase content as fibers cool down.^{29,30} The change of these peaks indicates that both the high temperature and strong electric field can synergistically increase the β -phase content of the ME-PVDF.

The β -phase content of each membrane was calculated from the FTIR spectra by applying

$$F(\beta) = \frac{A_\beta}{(K_\beta/K_\alpha)A_\alpha + A_\beta} \quad (1)$$

where $F(\beta)$ represents the β -phase content; A_α and A_β are the absorbances at 765 and 840 cm^{-1} , respectively, corresponding to the α - and β -phase material; and K_α and K_β are the absorption coefficients at the respective wavenumber. The value of K_α is $6.1 \times 10^4 \text{ cm}^2/\text{mol}$ and that of K_β is $7.7 \times 10^4 \text{ cm}^2/\text{mol}$.³⁰ The $F(\beta)$ values of the PVDF pellet and ME-PVDF are 0.36 ± 0.01 and 0.61 ± 0.04 , respectively. Therefore, the significant increase of the $F(\beta)$ value in the melt-electrospun membrane suggests that the melt-electrospinning process can promote the crystal formation of the β phase (Figure 1).

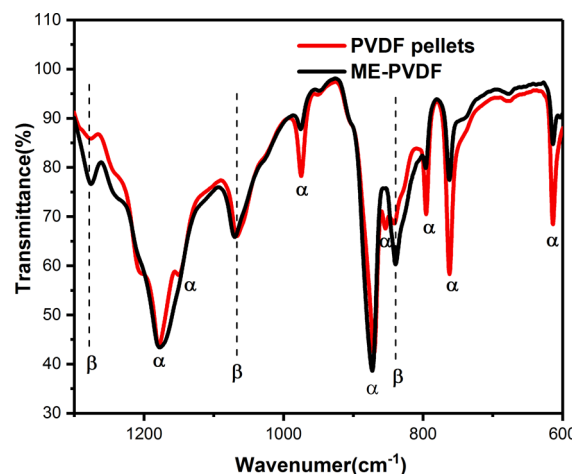


Figure 1. FTIR spectra of ME-PVDF and PVDF pellets.

The morphologies and porous structure of the polyethylene (PE) membrane, ME-PVDF, and ceramic nanoparticle-coated membranes were demonstrated by scanning electron microscopy (SEM) images (Figure 2). The PE membrane with a typical porous structure is shown in Figure 2e. The as-spun PVDF membrane presents a three-dimensional network structure with abundant open pores among the fibers (the inset in Figure 2a). ME-PVDF fibers show a rather smooth surface with an average diameter of $3.18 \pm 0.63 \mu\text{m}$. After sputter-coating, the PVDF fibers clearly showed increased roughness and the surface becomes more corrugated (Figure 2b–d). The increased surface roughness is hypothesized to be beneficial to the liquid electrolyte absorption, which will be further discussed in the latter part. As expected, the average fiber diameters increased to 3.28 ± 0.04 , 3.25 ± 0.08 , and $3.26 \pm 0.02 \mu\text{m}$ for the $\text{Al}_2\text{O}_3/\text{SiO}_2/\text{PVDF}$, $\text{Al}_2\text{O}_3/\text{PVDF}$, and SiO_2/PVDF membranes, respectively, corresponding to respective ca. 50, 35, and 40 nm ceramic nanoparticle coating layers. Although the fiber diameters increased after sputter-coating, all of the ceramic nanoparticle-coated membranes remain porous, suggesting that the open pores were unaffected by the deposition of nanoparticles (the inset in Figure 2b–d). The presence of ceramic nanoparticles on the surface of ME-PVDF fibers was verified from the energy-dispersive spectrum (EDS) (Figure 3). The uncoated PVDF membrane showed only signals for C and F, whereas Al and Si atoms can be observed from the Al_2O_3 and SiO_2 -coated membrane with respective 0.12 and 0.32 wt % content (inset table in Figure 3). The less Al content on the membrane could be due to the low-power setup during coating. As expected, both Al and Si atoms could be observed from the

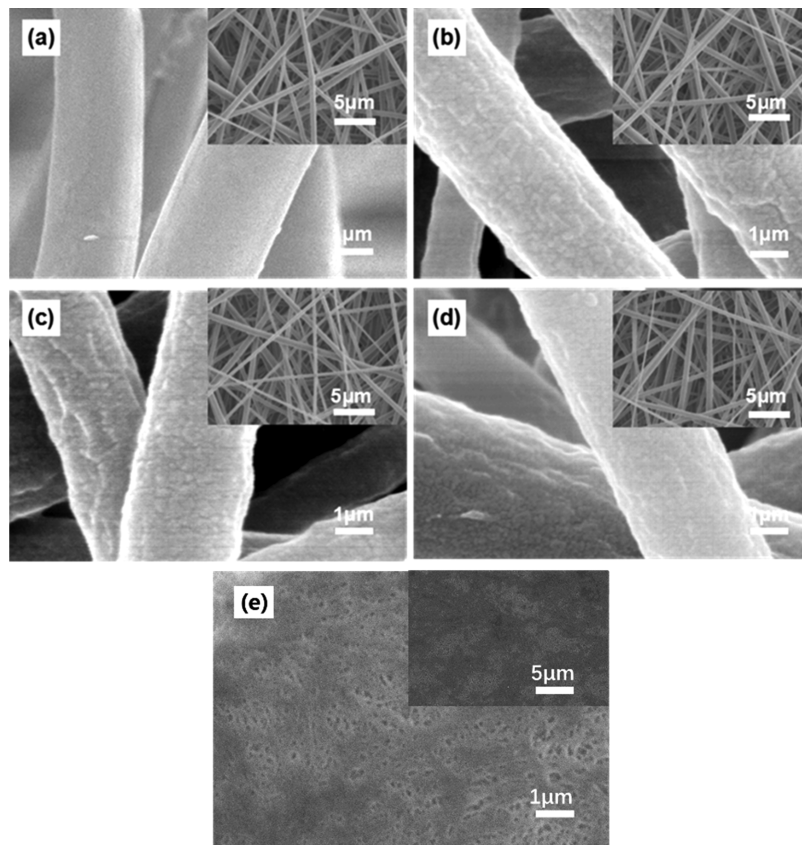


Figure 2. SEM images of (a) ME-PVDF, (b) $\text{Al}_2\text{O}_3/\text{SiO}_2/\text{PVDF}$, (c) $\text{Al}_2\text{O}_3/\text{PVDF}$, (d) SiO_2/PVDF composite membrane, and (e) PE membrane. Insets are low-magnification SEM images.

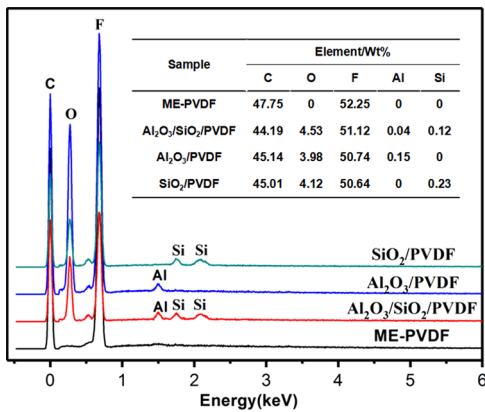


Figure 3. EDS elemental analysis of ME-PVDF, $\text{Al}_2\text{O}_3/\text{SiO}_2/\text{PVDF}$, $\text{Al}_2\text{O}_3/\text{PVDF}$, and SiO_2/PVDF composite nanofiber membranes.

$\text{Al}_2\text{O}_3/\text{SiO}_2/\text{PVDF}$ composite membrane, with respective 0.04 and 0.12 wt % content. Overall, the Al and Si contents on the $\text{Al}_2\text{O}_3/\text{SiO}_2/\text{PVDF}$ composite membrane are less than those on the respective $\text{Al}_2\text{O}_3/\text{PVDF}$ and SiO_2/PVDF membrane, as the coating time was halved for the $\text{Al}_2\text{O}_3/\text{SiO}_2/\text{PVDF}$ membrane.

2.2. Thermal Stability of the Membranes. The thermal stability of the separator membrane is a critical safety factor for lithium-ion batteries, as heat can be generated from continuous electrochemical reactions during charging and discharging within the battery. In addition, LIB has also been used at elevated temperature and/or at excessive discharge current, which requires high thermal stability that can withstand the temperature rise during service.³¹ Separators without satisfying

thermal stability tend to shrink or melt as the temperature increases, which can lead to short circuit or even explosion. The dimensional changes of polyethylene (PE) and ME-PVDF membranes after heating at 130 °C for 0.5 h are presented in Figure 4a. At a starting diameter of 18 mm, the PE membrane shrank drastically with more than 47% areal shrinkage, whereas the ME-PVDF membrane only showed approximately 11% areal shrinkage. The higher thermal stability of the ME-PVDF membrane is expected considering its higher melting point of 170 °C as compared to the 130 °C for PE. After coating with ceramic nanoparticles, no obvious shrinkage could be observed, which demonstrates that the deposited ceramic nanoparticles can significantly improve the thermal stability of the ME-PVDF membranes. The uniformly deposited ceramic nanoparticles can serve as a thermostable framework to resist the dimensional variation of PVDF separators at high temperatures.

The thermal stabilities of the ME-PVDF, $\text{Al}_2\text{O}_3/\text{SiO}_2/\text{PVDF}$, $\text{Al}_2\text{O}_3/\text{PVDF}$, and SiO_2/PVDF composite membranes were further characterized by thermogravimetric (TG) curves under a nitrogen atmosphere from 200 to 700 °C (Figure 4b). The TG curves of all four membranes showed almost no mass loss at temperatures below 400 °C, indicating high thermal stability of the PVDF fibrous membrane. The onset degradation temperature was used to identify the temperature at which the membranes start to degrade, which showed increased values from 415 °C for the uncoated membrane to 421 °C for both $\text{Al}_2\text{O}_3/\text{PVDF}$ and SiO_2/PVDF membranes and 445 °C for the $\text{Al}_2\text{O}_3/\text{SiO}_2/\text{PVDF}$ membrane. The increased onset temperature after ceramic nanoparticle coating indicates improved thermal stability, which is caused by the more thermally stable

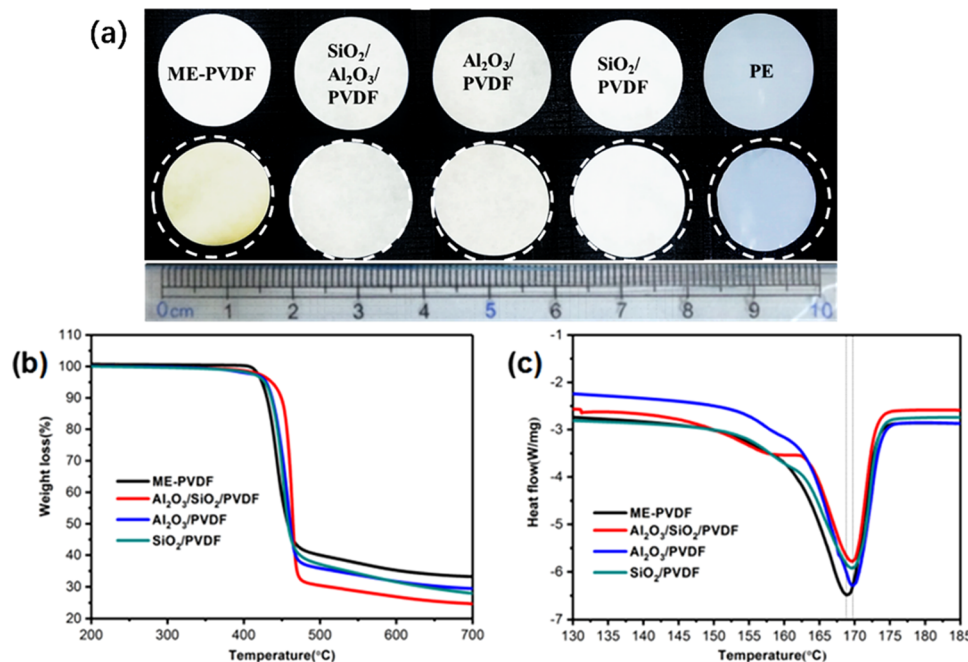


Figure 4. (a) Photographs of PE and ME-PVDF, $\text{Al}_2\text{O}_3/\text{SiO}_2/\text{PVDF}$, $\text{Al}_2\text{O}_3/\text{PVDF}$, and SiO_2/PVDF separator membranes before and after thermal treatment at $130\text{ }^\circ\text{C}$ for 2 h. (b) Thermogravimetric (TG) and (c) differential scanning calorimetry (DSC) curves of ME-PVDF, $\text{Al}_2\text{O}_3/\text{SiO}_2/\text{PVDF}$, $\text{Al}_2\text{O}_3/\text{PVDF}$, and SiO_2/PVDF membranes.

Table 1. Performance of ME-PVDF, $\text{Al}_2\text{O}_3/\text{SiO}_2/\text{PVDF}$, $\text{Al}_2\text{O}_3/\text{PVDF}$, SiO_2/PVDF , and PE Membranes

sample	thickness (μm)	bulk resistance (Ω)	ion conductivity (mS/cm, $25\text{ }^\circ\text{C}$)	electrolyte uptake (%)	porosity (%)
ME-PVDF	50	3.30	0.754	339.9	74.8
$\text{Al}_2\text{O}_3/\text{SiO}_2/\text{PVDF}$	50.1	1.21	2.055	366.2	61.8
$\text{Al}_2\text{O}_3/\text{PVDF}$	50.1	1.90	1.309	346.6	69.2
SiO_2/PVDF	50.1	2.63	0.946	369.6	62.4
PE	25	5.14	0.242	155.6	46.2

outer inorganic layer. However, the char residues at $700\text{ }^\circ\text{C}$ decreased with ceramic nanoparticle coating, showing respective values of 33.18, 29.41, 27.97, and 24.63% for ME-PVDF, $\text{Al}_2\text{O}_3/\text{PVDF}$, SiO_2/PVDF , and $\text{Al}_2\text{O}_3/\text{SiO}_2/\text{PVDF}$ membranes. The decreased char residues might be due to the generation of hydrogen fluoride during the decomposition of PVDF,³² which can easily react with Al_2O_3 and SiO_2 to lead to greater weight loss on the residual portion of the membranes. The melting temperature of all four PVDF membrane was investigated from DSC curves (Figure 4c), showing slightly increased values from $168.6\text{ }^\circ\text{C}$ for the pure ME-PVDF separator to 169.8 , 169.7 , and $169.7\text{ }^\circ\text{C}$ for $\text{Al}_2\text{O}_3/\text{SiO}_2/\text{PVDF}$, $\text{Al}_2\text{O}_3/\text{PVDF}$, and SiO_2/PVDF , respectively. The slightly increased melting temperature by the ceramic nanoparticle coating can be attributed to its interaction with PVDF fibers, which could restrict the polymer chain mobility.³³

In essence, ceramic nanoparticle coating can significantly improve the thermal stability of the ME-PVDF membranes, as indicated by less thermal shrinkage at $130\text{ }^\circ\text{C}$, increased melting temperature, and increased onset degradation temperature. Therefore, the ceramic nanoparticle-coated PVDF membrane can be better suited for lithium-ion battery applications.

2.3. Porosity and Electrolyte Uptake of Membranes.

Ionic conductivity represents the rate of lithium-ion transportation between the cathode and anode and is essential to the LIB performance. It is highly dependent on the porosity and affinity toward electrolyte. Compared to the commercial PE

separator, the ME-PVDF separator showed much higher porosity (74.8 vs 46.2%) (Table 1). The high porosity of the melt-electrospun membrane is expected due to the large interfiber spacings as previously observed from SEM imaging. In contrast, pores on the commercial PE separator were generated by hot stretching of the PE film, which can only create a limited number of open pores within the film structure. It is therefore concluded that melt-electrospinning can effectively fabricate highly porous membranes for LIB separators. Ceramic nanoparticle coating can slightly lower the porosity to around 62–69% due to the increased fiber diameters, but it is still significantly higher than the porosity of the PE membrane.

Apart from high porosity, good affinity between the separator and electrolyte is also critical for its electrochemical performance, as good wetting performance can facilitate the fast lithium-ion transport through a membrane. The wetting properties of the four membranes were evaluated by the liquid electrolyte spreading test (with $10\text{ }\mu\text{L}$ of electrolyte) and contact angle measurement (with $5\text{ }\mu\text{L}$ of electrolyte). The spreading of a drop of liquid electrolyte on the surface of ME-PVDF, $\text{Al}_2\text{O}_3/\text{SiO}_2/\text{PVDF}$, $\text{Al}_2\text{O}_3/\text{PVDF}$, SiO_2/PVDF , and PE membranes was recorded in Figure 6a, showing limited wetting on the PE membrane and fast spreading through the whole ME-PVDF, $\text{Al}_2\text{O}_3/\text{SiO}_2/\text{PVDF}$, $\text{Al}_2\text{O}_3/\text{PVDF}$, and SiO_2/PVDF membranes within 2 s. In addition, the liquid electrolyte contact angles (Figure 5b) on ME-PVDF, $\text{Al}_2\text{O}_3/\text{SiO}_2/\text{PVDF}$, $\text{Al}_2\text{O}_3/\text{PVDF}$,

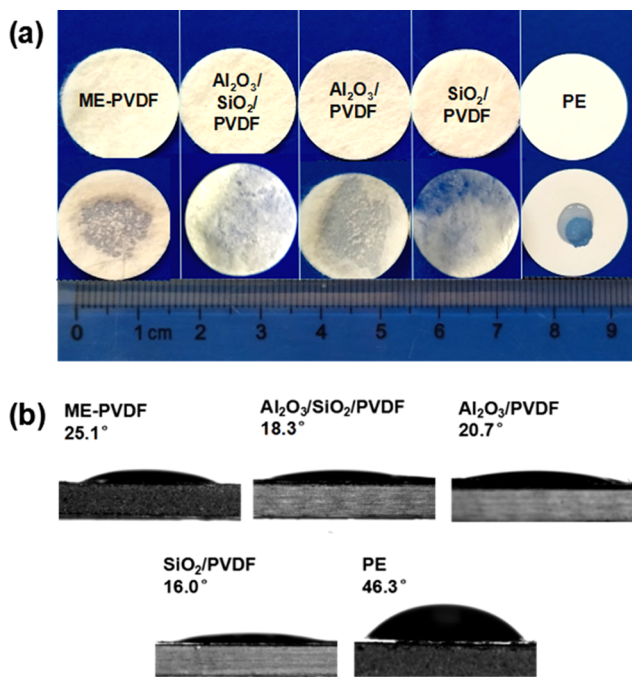


Figure 5. (a) Photographs of the wetting behavior. (b) Initial contact angles of the ME-PVDF, Al₂O₃/SiO₂/PVDF, Al₂O₃/PVDF, SiO₂/PVDF, and PE membranes with the liquid electrolyte.

SiO₂/PVDF, and PE membranes were quantified as 25.1, 18.3, 20.7, 16.0, and 46.3°, respectively. It is clear that the PVDF membrane showed much better wetting behavior than that of the PE membrane. This could be due to the existence of the

polar bonds (C—F) in the PVDF separator, therefore generating strong interaction with the polar electrolyte. In contrast, the PE membrane was made from hydrophobic polyolefin, which resulted in poor wettability with the polar liquid electrolyte.^{21,34} As expected, coating of the PVDF membrane with ceramic nanoparticles can further lower the contact angle due to the more polar Si—O and Al—O bonds. An electrolyte uptake test was conducted to further confirm the porosity and wettability of the membranes. Due to its low porosity and poor wettability with the liquid electrolyte, the PE membrane only showed 155.6% electrolyte uptake, which is less than half of the electrolyte uptake for the uncoated and coated PVDF membranes (346.6–369.6%) (Table 1). Combining with high porosity, high electrolyte uptake, and better wettability, the ceramic nanoparticle-coated membranes were expected to demonstrate improved electrochemical performance as compared to that of the commercial PE membrane or uncoated PVDF membrane.

2.4. Electrochemical Performance of Membranes. To determine the electrochemical performance of ME-PVDF and ceramic nanoparticle-coated membranes, electrochemical impedance spectra (EIS) were used to measure their ionic conductivity (Figure 6a,b). Based on eq 4, the ionic conductivities of the PE, ME-PVDF, Al₂O₃/SiO₂/PVDF, Al₂O₃/PVDF, and SiO₂/PVDF separators were calculated to be 0.242, 0.754, 2.055, 1.309, and 0.946 at room temperature, respectively. The ionic conductivity of the PVDF membrane is more than 3 times of that of the PE membrane, which can be explained by its higher porosity and better electrolyte affinity. The ceramic nanoparticle coating can further enhance the ionic conductivity due to the improved liquid electrolyte affinity by

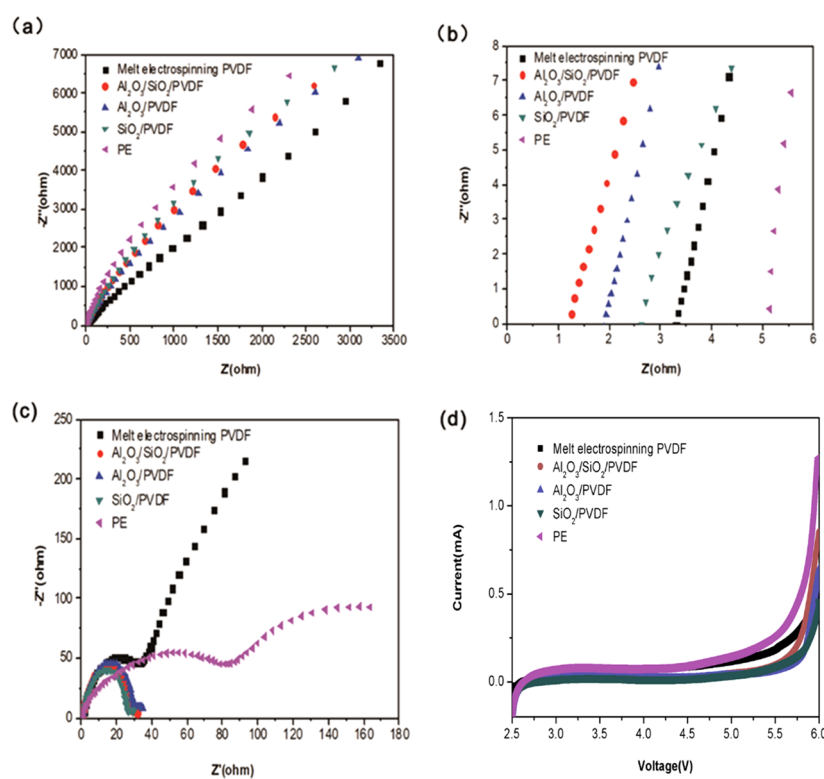


Figure 6. (a) Electrochemical impedance spectroscopy (EIS) profiles of ME- PVDF, Al₂O₃/SiO₂/PVDF, Al₂O₃/PVDF, SiO₂/PVDF, and PE membranes at 25 °C; (b) magnified image of the EIS profile; (c) AC impedance spectra, and (d) linear sweep voltammograms (LSV) of the different separators.

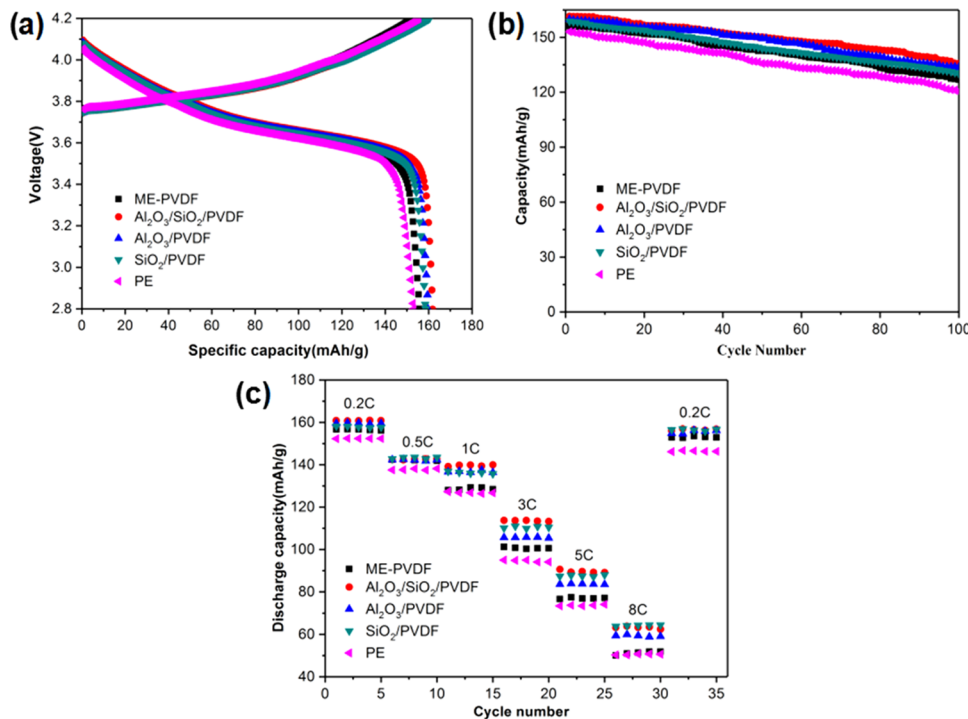


Figure 7. (a) Initial discharge capacity of the cells. (b) Battery cycle performance under 100 cycles of the 0.5C charge/discharge rate. (c) Rate capacity tests using the ME-PVDF, Al₂O₃/SiO₂/PVDF, Al₂O₃/PVDF, SiO₂/PVDF, and PE separators.

the more polar inorganic oxide nanoparticles. The compatibility of the lithium electrode with these membranes was also evaluated by EIS using a Li/membrane/Li symmetric cell. Figure 6c shows the Nyquist plots of the Li/separator/Li cell at the open-circuit potential. The interfacial impedance between the lithium electrode and PE membrane was $83\ \Omega$, which can be significantly reduced to 33, 29, 30, and $26\ \Omega$ for ME-PVDF, Al₂O₃/SiO₂/PVDF, Al₂O₃/PVDF, and SiO₂/PVDF membranes, respectively. The cell using ceramic nanoparticle-modified separators showed a reduced electrochemical resistance than that of the ME-PVDF separator, indicating smooth ion transport between the ceramic nanoparticle-coated separators and electrodes. Moreover, the SiO₂/PVDF membrane exhibited the smallest interfacial impedance and therefore had the best separator–electrode compatibility. This is consistent with a previous research that a very thin inorganic oxide layer can negate the interfacial impedance between the solid-state electrolyte and lithium metal, owing to the high binding energy between lithium and the alumina layer.³⁵

The electrochemical stability of the composite membranes was investigated by the linear sweep voltammetry (LSV) method. The electrochemical operating window of membranes is described in Figure 6d. The obtained result for the PE separator saturated with the liquid electrolyte indicated that oxidative decomposition happens at the potential of about 4.5 V (vs Li/Li⁺), which was ascribed to the low oxidative stability of the solvent components in the organic liquid electrolyte. Much higher oxidative potentials can be observed for the ceramic-modified separators. The Al₂O₃/SiO₂/PVDF separator was stable up to about 5.7 V electrochemically.

2.5. Battery Performance Analysis. The charge–discharge measurement can directly assess the effect of the ceramic nanoparticle-coated separators on the electrochemical performance of batteries. Figure 7a displays the initial charge–discharge profiles of Li/separator/LiNiCoMn cells cycled at

0.5C. The initial discharge capacities for the battery using PE and ME-PVDF membranes as separators were 153.0 and 156.1 mAh/g, respectively, which slightly increased to 161.5, 159.8, and 158.8 mAh/g for Al₂O₃/SiO₂/PVDF, Al₂O₃/PVDF, and SiO₂/PVDF separators, respectively. It can be observed that the LiNiCoMn electrode using the ceramic nanoparticle-coated separators exhibited a slightly higher initial reversible capacity and lower charge–discharge potential gap compared with those of the one using the PE separator, possibly due to the higher ionic conductivity of the ceramic nanoparticle-coated membranes (Figure 7a).

Figure 7b presents the cyclic stability of the LiNiCoMn cathode using various separators in the voltage range of 2.8–4.2 V under 0.5C rate at room temperature. Other than the slightly different initial capacity of the LiNiCoMn cathode for all five separators, as in Figure 7a, the fading rate also varies for these separators upon cycling. After 100 cycles, the discharge capacities of PE, ME-PVDF, Al₂O₃/SiO₂/PVDF, Al₂O₃/PVDF, and SiO₂/PVDF separators decreased to 120.5, 126.9, 135.6, 133.8, and 130.2 mAh/g, with specific capacity retention rates of 78.4, 81.3, 84.3, 83.7, and 82.0%, respectively. These results indicated that the Al₂O₃/SiO₂/PVDF separator had the best performance in the lithium-ion battery, which indicated that the affinity of the ceramic nanoparticles to the electrolyte and the increased β phase of PVDF can improve the electrochemical performance of separators.

Figure 7c depicts the rate capability of LiNiCoMn/separator/Li cells with PE, ME-PVDF, Al₂O₃/SiO₂/PVDF, Al₂O₃/PVDF, and SiO₂/PVDF separators at discharge currents from 0.2C to 8C. With the increase of the current rate, the ceramic nanoparticle-coated separators exhibited improved capacity retention compared with that of the PE separator. For instance, at the current density of 8C, the cell assembled with the PE separator maintained 49.8% capacity relative to the capacity at 0.2C, whereas the cell containing the Al₂O₃/SiO₂/PVDF

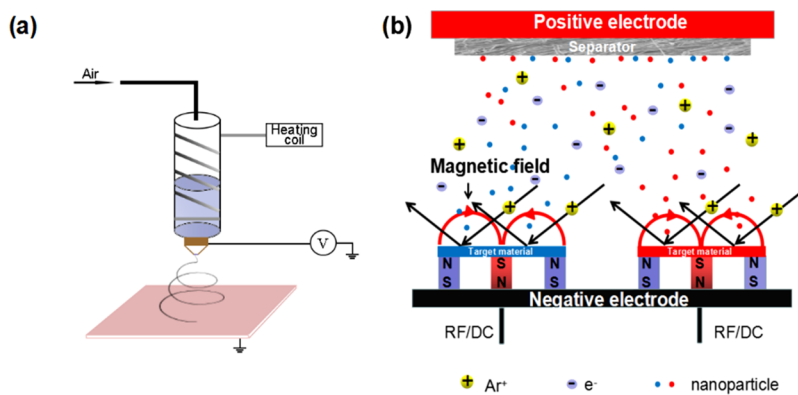


Figure 8. Schematics of (a) melt-electrospinning device and (b) magnetron sputtering deposition setup.

separator maintained 58.4%. The superior rate performance of the $\text{Al}_2\text{O}_3/\text{SiO}_2/\text{PVDF}$ separator can be attributed to better wetting ability and higher ion conductivity. In addition, the binder-free, thin-layer ceramic nanoparticles facilitated efficient ion transport without affecting the pore structure.

3. CONCLUSIONS

In summary, we prepared a ceramic nanoparticle-coated PVDF fiber membrane for lithium-ion batteries through melt-electrospinning (ME) and magnetron sputtering deposition (MSD). Under the synergistic effect of electric field and temperature of melt-electrospinning, the β phase of PVDF could improve effectively, thereby improving the ion conductivity. Compared to a commercial PE separator, the ceramic nanoparticle-coated separator exhibited good wettability, high ionic conductivity, and excellent thermal stability at high temperatures. The resulting lithium-ion battery containing the $\text{Al}_2\text{O}_3/\text{SiO}_2/\text{PVDF}$ composite separator exhibited high discharge capacity of 161.5 mAh/g and excellent cycling stability that retained a capacity of 135.6 mAh/g after 100 cycles, corresponding to 84.3% specific capacity retention rate. It is therefore concluded that the ceramic nanoparticle-coated ME-PVDF composite membranes are superior to PE membranes to be used as separators in lithium-ion batteries.

4. EXPERIMENTAL SECTION

4.1. Melt-Electrospinning and Ceramic Nanoparticle Coating of the PVDF Membrane. PVDF with a number-average molecular weight (M_n) of 5.5×10^4 g/mol and low viscosity (melt flow index (MFI) of 100 g/10 min at 230 °C) was purchased from Yijia Plastic Materials Co., Ltd. A homemade melt-electrospinning instrument (Figure 8a) was used to fabricate the PVDF nanofiber membrane. For a typical spinning experiment, a portion of 2.16 kg of PVDF pellets was loaded into a copper syringe ($\Phi = 24$ mm) with a blunt 0.8 mm spinneret. Melt-electrospinning was conducted at 220 °C to melt the PVDF in the syringe. A voltage of 20 kV was applied to the spinneret, and the spinning speed was set to 5 mL/h. A collecting plate covered by a piece of aluminum foil was used as a collector for fiber deposition.

After electrospinning, the melt-electrospun PVDF (ME-PVDF) separator was dried at 60 °C and then sputter-coated with ceramic nanoparticles using a magnetron sputtering setup (JZCK-420B, Shenyang Jingyi Research Technology Co. Ltd., China) (Figure 8b) from both silicon and aluminum targets (99.9% purity, Hefei Crystal Materials Technology Co., Ltd.). Direct current and radio-frequency magnetron sputtering

deposition techniques were used to deposit Al_2O_3 and SiO_2 layers, respectively. The sputter chamber was first vacuumed to 8.9×10^{-5} Pa before purging with working (Ar) and reactive (O_2) gases of 99.99% purity at different proportions (Table 2).

Table 2. Specific Sputtering Parameters Used for the Three ME-PVDF Membranes

sample	Ar/ O_2	power (W)
SiO_2/PVDF	4:1	45
$\text{Al}_2\text{O}_3/\text{PVDF}$	10:1	24
$\text{SiO}_2/\text{Al}_2\text{O}_3/\text{PVDF}$	7:1 SiO_2 : 45 Al_2O_3 : 24	

Sputter-coating was carried out under a gas pressure of 0.8 Pa with respective power listed in Table 2, and the coated ME-PVDF was named as SiO_2/PVDF and $\text{Al}_2\text{O}_3/\text{PVDF}$. For the composite ceramic nanoparticle-coated PVDF membrane ($\text{SiO}_2/\text{Al}_2\text{O}_3/\text{PVDF}$), the magnetron cosputtering method with two individual sputtering guns for SiO_2 and Al_2O_3 was employed. The specific sputtering parameters in Table 2 were selected based on the different oxidation properties of the silicon and aluminum targets. The thickness of the sputter-coated layer was determined using a quartz crystal microbalance (FTM107-A, Shanghai Taiyao Co. Ltd., China) as a catcher, and the thickness of the coated ceramic nanoparticle layers of all three membranes is around 200 nm. Immediately after sputter-coating, the ceramic nanoparticle-coated ME-PVDF membrane was further pressed using a hot press (Carver 4128, Carver Company, USA) at 75 °C and 10 000 psi for 10 min to ensure a flat surface for the lithium-ion battery separator application.

4.2. Characterization of the Ceramic Nanoparticle-Coated Membrane. Both melt-electrospun membranes and pellets were analyzed by Fourier transform infrared (FTIR) spectroscopy (Nicoletis10, Thermo Fisher Scientific Technology Co., Ltd., China) in the range of 600–4000 cm^{-1} to verify the PVDF crystalline-phase transformation. The membrane was sputter-coated with gold and examined by scanning electron microscopy (SU1510, Hitachi, Japan) at an accelerating voltage of 10 kV for the microscopic structure and morphology. The presence of inorganic elements of coated ceramic nanoparticles on the ME-PVDF membrane was investigated using energy-dispersive spectroscopy (EDS) (Quantax400, Bruker, German).

All membranes were thermally treated at 130 °C for 0.5 h to determine their respective areal thermal shrinkage (A), which was calculated using the following equation

$$A (\%) = \frac{S_0 - S_T}{S_0} \times 100\% \quad (2)$$

where S_0 and S_T refer to the area of the membrane before and after thermal treatment, respectively.

Differential scanning calorimetry (DSC) (TA-Q200, Waters, China) was used to measure the thermal stability of membranes from 20 to 200 °C with a heating rate of 10 °C/min under a nitrogen atmosphere at a flow rate of 20 mL/min. Thermal gravimetric analysis (TGA Q500, USA Waters Industry) of the membranes was conducted from 20 to 700 °C under a N₂ atmosphere at a heating rate of 10 °C/min.

The porosity of the membrane was calculated according to the following equation

$$P (\%) = \frac{M_{BuOH}/\rho_{BuOH}}{M_{BuOH}/\rho_{BuOH} + M_m/\rho_p} \times 100\% \quad (3)$$

where M_m and M_{BuOH} represent the masses of the membrane before and after absorbing *n*-butanol, respectively, while ρ_{BuOH} and ρ_p represent the densities of *n*-butanol and PVDF, respectively.

The electrolyte wettability of the membranes was examined by the electrolyte spreading test. About 10 μL of electrolyte (1 M LiPF₆ in ethylene carbonate, dimethyl carbonate, methyl ethyl carbonate EC/DMC/EMC, 1:1:1, by volume) was dropped onto the membrane in an argon-filled glovebox, and the electrolyte spreading was captured after 15 s. An optical contact angle meter (DCAT-21, GER Dataphysica Industry) was used to quantify the spreadability by taking the droplet contact angle of liquid electrolyte (with 5 μL of electrolyte) just dripped onto the membranes at room temperature. The electrolyte uptake was determined according to the following equation

$$\text{uptake (\%)} = \frac{W - W_0}{W_0} \times 100\% \quad (4)$$

where W_0 and W are the wet weights of the membrane before and after completely absorbing liquid electrolyte.

4.3. Electrochemical Performance of the Ceramic Nanoparticle-Coated Membrane. The ionic conductivity of membranes was determined by electrochemical impedance spectroscopy (EIS) using a CHI 660E electrochemical workstation (CH Instruments, Shanghai, China). The membranes were saturated with about 30 μL of liquid electrolyte, sandwiched between two stainless steel plates, and assembled as a coin cell (CR2032). EIS analysis was performed at a frequency range of 0.1–10⁶ Hz. The ionic conductivities were calculated by the following equation

$$\sigma = L/(R_b \times S) \quad (5)$$

where L and R_b represent the thickness and bulk resistance of the membrane, respectively, and S is the area of the stainless steel electrode.

A lithium symmetric cell was assembled by sandwiching the electrolyte-saturated membrane between two lithium electrodes in a coin cell and was used to characterize the LIB interfacial charge-transfer resistance by EIS at a frequency range of 0.01–10⁶ Hz. The electrochemical stability window of the membranes was measured by linear sweep voltammetry (LSV). The membrane was sandwiched between a stainless steel working electrode and a lithium metal counterelectrode. The LSV test was carried out at a scan rate of 10 mV/s over a voltage range 2.5–6.0 V vs Li⁺/Li.

The performance of the PVDF membrane as a lithium-ion battery separator was tested in a coin cell assembly using metallic Li (Shenzhen Kejing Zhida Technology Co. Ltd., China) as an anode, an active material composition of 94.2 wt % LiNiCoMnO₂ (Shenzhen kejing Zhida Technology Co. Ltd, China) as a cathode, and approximately 30 μL of electrolyte solution (1 M LiPF₆ in EC/DMC/EMC, 1:1:1, by volume). Five different membranes were tested for comparison: separator PE as a control (20 μm thick) and ME-PVDF, Al₂O₃/SiO₂/PVDF, Al₂O₃/PVDF, and SiO₂/PVDF (the thickness for all PDVF membranes is 25 μm). The coin cells were assembled in a glovebox (Mbraun, Germany) filled with argon gas. The charge and discharge cycling tests on cells were performed at 0.5C with a battery test equipment (CT-3008W-5V1nA-S4, Shenzhen Neware Technology Limited, China). Cells were charged to 4.2 V and discharged to 2.8 V at current rates of 0.5C, 1.0C, 2.0C, 5.0C, 8.0C, and 10.0C for the measurement of rate capacity.

■ AUTHOR INFORMATION

Corresponding Author

*E-mail: flhuang@jiangnan.edu.cn

ORCID

Fenglin Huang: 0000-0001-8108-8822

Notes

The authors declare no competing financial interest.

■ ACKNOWLEDGMENTS

We are grateful to the Jiangsu Key R&D Program (BE2017060, BE2016707), the China Postdoctoral Science Foundation (169483), and the 111 Project (B17021).

■ REFERENCES

- Tarascon, J.-M.; Armand, M. Issues and challenges facing rechargeable lithium batteries. *Mater. Sustainable Energy* **2010**, *171–179*.
- Zhang, S. S. A review on the separators of liquid electrolyte Li-ion batteries. *J. Power Sources* **2007**, *164*, 351–364.
- Fu, K.; Cheng, J.; Li, T.; Hu, L. Flexible Batteries: From Mechanics to Devices. *ACS Energy Lett.* **2016**, *1*, 1065–1079.
- Hwang, K.; Kwon, B.; Byun, H. Preparation of PVdF nanofiber membranes by electrospinning and their use as secondary battery separators. *J. Membr. Sci.* **2011**, *378*, 111–116.
- Li, Y.; Tang, S.; Pan, M.-W.; Zhu, L.; Zhong, G.-J.; Li, Z.-M. Polymorphic extended-chain and folded-chain crystals in poly(vinylidene fluoride) achieved by combination of high pressure and ion-dipole interaction. *Macromolecules* **2015**, *48*, 8565–8573.
- Satyanarayana, K. C.; Bolton, K. Molecular dynamics simulations of α-to β-phase (vinylidene fluoride) phase change by stretching and poling. *Polymer* **2012**, *53*, 2927–2934.
- Lu, F.; Hsu, S. Study of the crystallization behavior of poly(vinylidene fluoride) from melt under the effect of an electric field. *Macromolecules* **1986**, *19*, 326–329.
- Pan, J.-L.; Zhang, Z.; Zhang, H.; Zhu, P.-P.; Wei, J.-C.; Cai, J.-X.; Yu, J.; Koratkar, N.; Yang, Z.-Y. Ultrathin and Strong Electrospun Porous Fiber Separator. *ACS Appl. Energy Mater.* **2018**, *1*, 4794–4803.
- Miao, Y.-E.; Zhu, G.-N.; Hou, H.; Xia, Y.-Y.; Liu, T. Electrospun polyimide nanofiber-based nonwoven separators for lithium-ion batteries. *J. Power Sources* **2013**, *226*, 82–86.
- Kang, D.-W.; Kim, J.-K. Characterization of fibrous gel polymer electrolyte for lithium polymer batteries with enhanced electrochemical properties. *J. Electroanal. Chem.* **2016**, *775*, 37–42.
- Subbiah, T.; Bhat, G.; Tock, R.; Parameswaran, S.; Ramkumar, S. Electrospinning of nanofibers. *J. Appl. Polym. Sci.* **2005**, *96*, 557–569.
- Lyons, J.; Li, C.; Ko, F. Melt-electrospinning part I: processing parameters and geometric properties. *Polymer* **2004**, *45*, 7597–7603.

- (13) Hutmacher, D. W.; Dalton, P. D. Melt electrospinning. *Chem. - Asian J.* **2011**, *6*, 44–56.
- (14) Fu, Q.; Lin, G.; Chen, X.; Yu, Z.; Yang, R.; Li, M.; Zeng, X.; Chen, J. Mechanically Reinforced PVdF/PMMA/SiO₂ Composite Membrane and Its Electrochemical Properties as a Separator in Lithium-Ion Batteries. *Energy Technol.* **2018**, *6*, 144–152.
- (15) Nho, Y.-C.; Sohn, J.-Y.; Shin, J.; Park, J.-S.; Lim, Y.-M.; Kang, P.-H. Preparation of nanocomposite γ -Al₂O₃/polyethylene separator crosslinked by electron beam irradiation for lithium secondary battery. *Radiat. Phys. Chem.* **2017**, *132*, 65–70.
- (16) Xue, L.; Xu, G.; Li, Y.; Li, S.; Fu, K.; Shi, Q.; Zhang, X. Carbon-Coated Si Nanoparticles Dispersed in Carbon Nanotube Networks As Anode Material for Lithium-Ion Batteries. *ACS Appl. Mater. Interfaces* **2013**, *5*, 21–25.
- (17) Yang, C.; Tong, H.; Luo, C.; Yuan, S.; Chen, G.; Yang, Y. Boehmite particle coating modified microporous polyethylene membrane: a promising separator for lithium ion batteries. *J. Power Sources* **2017**, *348*, 80–86.
- (18) Zhu, X.; Jiang, X.; Ai, X.; Yang, H.; Cao, Y. TiO₂ ceramic-grafted polyethylene separators for enhanced thermostability and electrochemical performance of lithium-ion batteries. *J. Membr. Sci.* **2016**, *504*, 97–103.
- (19) Luo, X.; Liao, Y.; Zhu, Y.; Li, M.; Chen, F.; Huang, Q.; Li, W. Investigation of nano-CeO₂ contents on the properties of polymer ceramic separator for high voltage lithium ion batteries. *J. Power Sources* **2017**, *348*, 229–238.
- (20) Song, J.; Ryoo, M.-H.; Son, B.; Lee, J.-N.; Lee, D. J.; Lee, Y. M.; Choi, J. W.; Park, J.-K. Co-polyimide-coated polyethylene separators for enhanced thermal stability of lithium ion batteries. *Electrochim. Acta* **2012**, *85*, 524–530.
- (21) Liang, X.; Yang, Y.; Jin, X.; Cheng, J. Polyethylene oxide-coated electrospun polyimide fibrous separator for high-performance lithium-ion battery. *J. Mater. Sci. Technol.* **2016**, *32*, 200–206.
- (22) Bicy, K.; Suriyakumar, S.; Anu, A.; Kalarikkal, N.; Stephen, A. M.; Geethamma, V.; Rouxel, D.; Thomas, S.; et al. Highly lithium ion conductive, Al₂O₃ decorated electrospun P (VDF-TrFE) membranes for lithium ion battery separators. *New J. Chem.* **2018**, *42*, 19505–19520.
- (23) Jeong, H.-S.; Hong, S. C.; Lee, S.-Y. Effect of microporous structure on thermal shrinkage and electrochemical performance of Al₂O₃/poly (vinylidene fluoride-hexafluoropropylene) composite separators for lithium-ion batteries. *J. Membr. Sci.* **2010**, *364*, 177–182.
- (24) Shin, W.-K.; Kim, D.-W. High performance ceramic-coated separators prepared with lithium ion-containing SiO₂ particles for lithium-ion batteries. *J. Power Sources* **2013**, *226*, 54–60.
- (25) Zuo, J.; Keil, P.; Grundmeier, G. Synthesis and characterization of photochromic Ag-embedded TiO₂ nanocomposite thin films by non-reactive RF-magnetron sputter deposition. *Appl. Surf. Sci.* **2012**, *258*, 7231–7237.
- (26) Zhang, X.; Qiu, Y.; Tan, Z.; Lin, J.; Xu, A.; Zeng, Y.; Moore, J.; Jiang, J. Effect of Al content on structure and properties of TiAlCN coatings prepared by magnetron sputtering. *J. Alloys Compd.* **2014**, *617*, 81–85.
- (27) Zhang, Y.; Feng, F.; Shi, K.; Lu, H.; Xiao, S.; Wu, W.; Huang, R.; Qu, T.; Wang, X.; Wang, Z.; Han, Z. H. Surface morphology evolution of CeO₂/YSZ (001) buffer layers fabricated via magnetron sputtering. *Appl. Surf. Sci.* **2013**, *284*, 150–154.
- (28) Li, J.; Meng, Q.; Li, W.; Zhang, Z. Influence of crystalline properties on the dielectric and energy storage properties of poly (vinylidene fluoride). *J. Appl. Polym. Sci.* **2011**, *122*, 1659–1668.
- (29) Janakiraman, S.; Surendran, A.; Ghosh, S.; Anandhan, S.; Venimadhav, A. A new strategy of PVDF based Li-salt polymer electrolyte through electrospinning for lithium battery application. *Mater. Res. Express* **2019**, *6*, No. 035303.
- (30) Sajkiewicz, P.; Wasiak, A.; Gocłowski, Z. Phase transitions during stretching of poly (vinylidene fluoride). *Eur. Polym. J.* **1999**, *35*, 423–429.
- (31) Kundu, M.; Costa, C. M.; Dias, J.; Maceiras, A.; Vilas, J. L.; Lanceros-Méndez, S. On the relevance of the polar β -phase of poly (vinylidene fluoride) for high performance lithium-ion battery separators. *J. Phys. Chem. C* **2017**, *121*, 26216–26225.
- (32) Baginska, M.; Blaiszik, B. J.; Merriman, R. J.; Sottos, N. R.; Moore, J. S.; White, S. R. Autonomic shutdown of lithium-ion batteries using thermo-responsive microspheres. *Adv. Energy Mater.* **2012**, *2*, 583–590.
- (33) Campos, J. S. C.; Ribeiro, A. A.; Cardoso, C. X. Preparation and characterization of PVDF/CaCO₃ composites. *Mater. Sci. Eng., B* **2007**, *136*, 123–128.
- (34) Bhute, M. V.; Kondawar, S. B. Electrospun poly (vinylidene fluoride)/cellulose acetate/AgTiO₂ nanofibers polymer electrolyte membrane for lithium ion battery. *Solid State Ionics* **2019**, *333*, 38–44.
- (35) Han, X.; Gong, Y.; Fu, K. K.; He, X.; Hitz, G. T.; Dai, J.; Pearse, A.; Liu, B.; Wang, H.; Rubloff, G.; et al. Negating interfacial impedance in garnet-based solid-state Li metal batteries. *Nat. Mater.* **2017**, *16*, 572–579.